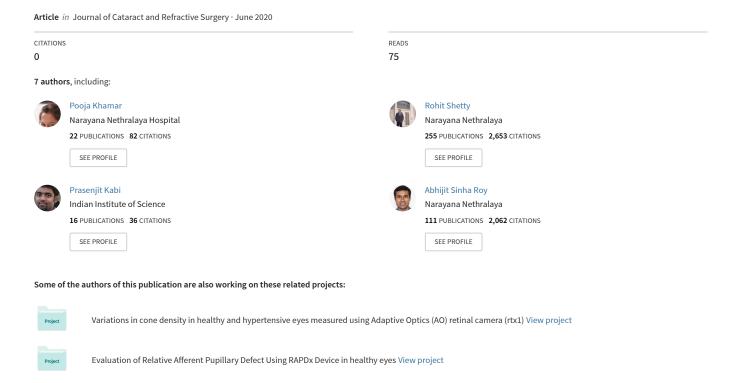
Quantitative shadowgraphy of aerosol and droplet spread during oscillatory motion of the microkeratome amidst COVID-19 and other infectious diseases



Quantitative shadowgraphy of aerosol and droplet spread during oscillatory motion of the microkeratome amidst COVID-19 and other infectious diseases

Running title: Aerosol and droplet with microkeratome

Pooja Khamar, MD, PhD¹
Rohit Shetty, MD, PhD, FRCS¹
Nikhil Balakrishnan, MD¹
Prasenjit Kabi, PhD²
Durbar Roy, MTech²
Saptarshi Basu, PhD²
Abhijit Sinha Roy, PhD^{3,#}

¹Department of Cornea and Refractive surgery, Narayana Nethralaya, Bangalore, India; ²Department of Mechanical Engineering, Indian Institute of Science, Bangalore, India; ³Imaging, Biomechanics and Mathematical Modeling solutions, Narayana Nethralaya Foundation, Bangalore, India

Acknowledgements: We would like to acknowledge the Defense Research and Development Organization, India Chair Professorship for funding.

Disclosures: None

Key words: aerosol, droplets, microkeratome, LASIK, PRK, SMILE, COVID-19, SARS-CoV-2

*Corresponding author: Dr. Abhijit Sinha Roy, Narayana Nethralaya, #258/A Hosur Road, Health City, Bommasandra, Bangalore-560099, India.

Abstract

Purpose: To quantify the atomization of liquid over the cornea during flap creation using

microkeratome using high speed shadowgraphy

Setting: Laboratory investigational study

Design: Laboratory study

Method: In an experimental set-up, flap creation was performed on enucleated goat's eyes (n=8)

mounted on a stand using One-Use Plus SBK Moria microkeratome (Moria SA, Antony, France)

to assess the spread of aerosols and droplets using high speed shadowgraphy. Two conditions

were computed. A constant air flow assumed uniform air velocity throughout the room. A

decaying jet assumed that local air velocity at the site of measurements was smaller than the exit

velocity from the air duct.

Results: With the advancement of the microkeratome across the wet corneal surface the

atomization of balanced salt solution was recorded on shadowgraphy. The minimum droplet size

was ~90 μm. The maximum distance traversed was ~1.8 m and ~1.3 m assuming a constant air

flow (setting of refractive surgery theater) and decaying jet condition (setting of an operating

theater with air-handling unit), respectively.

Conclusion: The microkeratome assisted LASIK flap creation does appear to cause spread of

droplets. The droplet diameters and velocities did not permit the formation of aerosols.

Therefore, the risk of transmission of the virus to the surgeon and surgical personnel due to the

microkeratome procedure appears to be low.

2

Introduction

As of late May 2020, the COVID-19 pandemic had affected 215 countries worldwide with over 6 million positive patients and over 350,000 deaths. Infectious disease outbreaks are challenging since they can overburden the health-care facilities. The severe acute respiratory syndrome coronavirus 2 (SARS-CoV-2) is a viral infection caused by the novel Coronavirus. It has rapidly become the world's 6th public health emergency of international concern (PHEIC). The primary route of transmission of SARS-CoV-2 is via direct contact with the respiratory secretions and droplets of an infected person. The virus may survive on different surfaces for days and heighten the risk of transmission. Airborne transmission of a disease is defined as the transmission of infection via large droplets over short distances or via aerosols (smaller droplets) over large distances.

Various surgical procedures performed by Ophthalmologists may generate aerosols from viral shedding areas, such as the conjunctiva and tears. It has been reported that the SARS-CoV-2 can be detected in the conjunctival swabs of COVID-19 patients. Though there are no conclusive reports on transmission of the virus from the conjunctiva and tears, all precautions while examining and operating on patients with ophthalmic indications should be taken as many patients may be asymptomatic carriers of the virus. Laser-in-situ-keratomileuses (LASIK) is one of the most commonly performed ophthalmic surgeries worldwide. The LASIK flap can be created using a microkeratome which typically oscillates the blade at 6,000 to 15,000 cycles per minute, and produces aerosol when it comes in contact with a wet ocular surface. High frequency oscillations are known to generate aerosols.

The droplets and aerosols can be studied using the schlieren and shadowgraph imaging technique although the former is more complicated to implement in clinical procedures such as the microkeratome. In shadowgraphy, a bright strobe light emitting diode (LED) source is used to cast the shadow of the fast-moving droplets and aerosols onto the sensor of an ultra-high speed camera. Therefore, we quantified the aerosol and droplet generation during flap creation using the Moria One-Use Plus SBK microkeratome (Moria SA, Antony, France) and assessed their trajectory using high speed shadowgraphy and fluid mechanics principles.

Methods

The experiment was conducted on enucleated goat eyes (n=8) to avoid experimenting on cadaveric human eyeballs as per the guidelines laid down by the Global eye bank association (GAEBA) and Eye bank association of India (EBAI), which prohibited retrieval of cadaveric eyes during the ongoing pandemic for the safety of healthcare personnel. ¹⁵ The goat eyes have been widely utilized for training and research purposes in ophthalmology. ¹⁶ The clarity of the cornea in the enucleated goat eye was inspected visually. The goat eye was inflated by injecting with balanced salt solution (BSS; Beaver-Visitec International, Oxford, UK) though the optic nerve. After the initial preparation, the goat eye was mounted on a base such that the whole cornea, limbus and some part of sclera was completely visible to the operating surgeon for ease of surgical maneuvering (Figure 1a). The One-Use Plus SBK Moria microkeratome (Moria SA, Antony, France) was used to create a corneal flap on the goat's eye. We aimed for a standard flap which was 9.0-mm in diameter and 130 µm in depth with a nasal hinge using A-1 ring. The flap creation was attempted once a vacuum of 140mm Hg was achieved. BSS (0.2 ml) was used to wet the corneal surface prior to flap creation (Figure 1b). A new blade was used for each goat

eye. The temperature of the experiment room was set at 21°C using a room air-conditioner and the humidity was set in the range of 40-50% using a de-humidifier. These settings were the same as the ones used in the operating rooms meant for refractive surgery in our hospital. Our refractive operating rooms also included room air-conditioners and de-humidifier.

Shadowgraphy technique was used to visualize the droplets generated during flap creation with the microkeratome. For objects in motion, an appropriate choice of camera shutter speed was chosen to avoid blurred images. Figure 2a shows a high-speed CCD camera (Mini UX100; Photron USA Inc., San Diego, USA) on the right positioned opposite to a high-power LED source (Constellation 120; Veritas, USA) on the left. Two sets of macro lenses were used for imaging with the camera. A 50 mm lens (Nikkor AF F1.4; Nikon Imaging Japan Inc., Tokyo, Japan) was used to visualize the trajectory of the droplets emanating from the site of incision. A 100 mm lens (ATX PRO F2.8D; Kenko Tokina Co. Ltd., Tokyo, Japan) was used to image and estimate the droplet size distribution (Figure 2b). In this case, the aperture was maintained at f/32 for maximum depth field. The surgical procedure was performed in a way such that the direction of primary trajectory of the aerosols and droplets was perpendicular to the lens camera. This allowed the trajectory to remain within the given depth of focus of the imaging system. The acquisition rate of the camera was set at 500 fps and the shutter speed was set at 1/18000 second.

To estimate the spread of the aerosols and droplets, the size distribution was extracted from the images using the "analyze particles" plugin of ImageJ (open source image JAVA based image processing platform) and used for further calculations. A simple one-dimensional analysis was used. During the course of flap cut, a droplet of diameter D µm ejected with a velocity u_d

(horizontal component) was measured. Operating theatres other than the ones used for refractive surgery have high efficiency air filtration systems which create a flow of air around this droplet. Thus, the profile of the air flow may be a constant airflow (such as the refractive surgery operating theater) or a decaying jet (our other operating theaters) based on the relative positioning of the air duct and the operating table. In a decaying jet, it was assumed that the operating table was located at a horizontal distance (l_o) from the air duct. Then, the airflow velocity (u_{air}) was modeled as:

$$u_{air} = \frac{3u_{in} \times d_{duct}}{K \times l_0}, l_0 \approx \frac{3 \times d_{duct}}{K}$$
[1]

where u_{in} was the exit velocity from the duct, K (~0.457) was the turbulent entrainment constant and d_{duct} was the diameter of the duct. ^{17,18} Thus, equation 1 provided a measure of the local airflow velocity at the operating table. In a constant airflow scenario, u_{air} was equal to u_{in} throughout the operating room. The appropriate governing drag equation for the droplet is given below:

$$\frac{du_d}{dt} = \frac{18}{r^2} \frac{\mu_f}{\rho_d} \frac{u_{rel}(u_{air} - u_d)}{u_{rel}}$$
[2]

where $u_{rel} = \sqrt{(u_{air} - u_d)^2 + v_d^2}$, r=D/2, v_d is the settling rate of the droplet, μ_f is the viscosity of air (=18.37×10⁻⁶ Pa.sec), ρ_f is the density of air (=1.184 kg/m³), ρ_d is the density of droplet (=997 kg/m³) and g is the acceleration due to gravity (=9.81 m/sec²). The droplet evaporates as well as settles due to gravity simultaneously. The evaporation timescale can be estimated from the D² law ¹⁹ while the appropriate settling rate (v_d) from the Stokes equation is:

$$v_{d} = (\rho_{d} - \rho_{f}) \frac{gD^{2}}{18\mu_{f}}$$
 [3]

The calculation assumes that the point of surgical incision is at \sim 1 m height from the operating theater floor. Thus, the timescale of droplet settling was obtained from equation 3 as:

$$t_{s} = \frac{1}{v_{d}} = \frac{18\mu_{f}}{(\rho_{d} - \rho_{f})gD}$$
 [4]

For the constant airflow condition, the value of u_{air} was estimated to be ~ 0.6 m/s which was as per the certified inspection report of the operating theatres at the Narayana Nethralaya eye hospital. For the decaying jet condition, u_{in} was assumed as ~ 0.6 m/sec. The rated capacity of the air-handling units in our operating theaters (3 in number) ranged from 2364 to 2653 ft³/min and the number of air changes per hour was not less than 40. The properties of air at a temperature of 23°C were used in all the equations.

Results

With the advancement of the microkeratome through the stroma, the atomization of water was visible on the shadowgraphy image (Figures 3a-b and video in supplementary model). Most of the droplets were generated in a direction which was at an angle of 90° to the direction of advancement of the microkeratome over the cornea. Shadowgraphy in the direction of advancement of the microkeratome had technical challenges since the surgeon hands and microkeratome itself blocked the camera field of view. Figure 4a shows the setup imaged using the 50 mm lens before the start of the flap cut. The droplet trajectories were visualized in Figure 4b by superimposition of 50 sequential images. It was apparent that the smaller droplets travelled farther from the point of ejection. For example, a droplet of diameter 386 µm travelled 26 mm in the horizontal direction while a droplet of diameter 578 µm travelled only 13 mm in the same direction (both measured at the same vertical depth of 0.01 m from the point of ejection). These distances were calculated assuming that there was no air circulation (i.e., uair=uin=0.0) in the theater. Given the limitation of the 50 mm lens in imaging the smaller droplets, a 100 mm lens

was used for shadowgraphy as shown in Figure 4c. The droplet size distribution was extracted from the JAVA based image processing platform and is presented in Figure 4d.

The most prevalent droplet diameters were in the range of 90 to 150 μ m while droplets larger than 500 μ m were very few in number. We have computed the maximum traversal of a droplet based a constant air flow and decaying jet. As shown in Figure 4e, the value of x (axial distance) showed a monotonic decrease with increasing diameter (D) of the droplet for both the conditions. Naturally, the constant air flow resulted in greater axial distance for the same droplet diameter. A power law fit showed the distance travelled by the droplets in case of a decaying jet as $x\approx17604\times D^{-2.11}$ while the same for constant airflow was $x\approx52584\times D^{-2.25}$. The maximum distance traversed was ~1.8 m and ~1.3 m assuming a constant air flow (setting of refractive surgery theater) and decaying jet condition (setting of an operating theater with air-handling unit), respectively. The value of u_d used for these calculations was ~0.252 m/s and was estimated from the high-speed shadowgraphs.

Discussion

An effective risk assessment of different surgical procedures can help mitigate the risk of transmission to health care professionals. Theoretically, there is always a risk of transmission of infectious diseases via aerosols and droplets. Wong et al. and Darcy et al. demonstrated that aerosol generation in experimental models of phacoemulsification and vitrectomy. ^{20,21} However, the possibility of aerosol generation during LASIK flap creation has not yet been explored. The principle of shadowgraph is based on the bending of light around higher density objects (in this case liquid droplets in air) such that the image projected on the screen (in this case the camera

sensor) is dark. ²² Shadowgraphy when combined with imaging at a high speed (500 fps and 1/40000s of shutter speed) and with a high resolution camera (24 μ m per pixel) can capture particle sizes as small as 50 μ m. It is known that droplets in the size range of 0.2-500 μ m mostly contribute to the spread of airborne diseases. ²³ Thus, it is critical to estimate the distance travelled by the ejected droplets in order to ascertain their potential as infection vectors. The horizontal distance (x) travelled by the droplet is dependent on both the evaporation time scales and the settling time scales, and is finally determined from the smaller of the two quantities. Since the smallest detected droplet diameter was ~90 μ m, the process was controlled primarily by the settling timescale. Since the smallest droplet diameter detected was greater than 24 μ m, it was highly unlikely that any droplet smaller than 24 μ m up to 10 μ m in diameter existed since a diameter of 10 μ m is usually considered as the upper limit for aerosol. However, the calculations presented here did not account for the clustering effect observed in sprays. ²⁴

In our experimental model, we used BSS for lubricating the cornea prior to the flap creation by the microkeratome. The wetting of the corneal surface may be a contributory factor in aerosol generation. Thus, aerosol and droplet generation were observed during the advancement of the microkeratome over the corneal surface. We believe that it was due to the atomization of the BSS secondary to the oscillatory movements within the microkeratome. Lubricating the corneal surface before use of microkeratome for flap creation is essential in order to prevent the epithelial erosions. ²⁵ Thus, this may be a potential source of viral transmission from an asymptomatic patient to the operating surgeon during the procedure.

Most of the droplet diameters ranged from 90-900 µm during microkeratome assisted LASIK (Figure 4d). Droplets smaller than 90 µm were non-existent. Although the initial size of the

droplets was too large to be classified as an aerosol, subsequent viscous shear against air may reduce them to about 0.1 to 0.3 times the original size. ²⁶ Given the droplet size distribution and their velocities, it is highly probable that they will settle on a surface before they evaporate in smaller sizes. Thus, the surgeons and other personnel in the surgical area need to take adequate measures to avoid contact with the settled droplets. It should be noted that Figure 4e does not provide the distribution of volume of BSS distributed over the range of droplets. Nonetheless, the larger droplets tend to settle faster, travel less distance and have lower risk of aerosolization.

An understanding of the stochastic nature of droplet creation from the motion of the microkeratome is required. Atomization of the BSS film on the corneal surface depends on several factors, e.g., frequency of oscillations, speed of advancement of the blade in the direction of flap cut, thermo-physical properties of the fluid, make of the device. Nonetheless, our experiments showed that the droplet diameters were bounded between 900 and 1200 µm (Figure 4e) in the all the captured frames of the shadowgraphy videos. For each eye, as many as 1000 frames were captured over a 2 second period. However, the distribution of the droplet sizes between the frames differed sharply due to the *stochastic* (random) nature of droplet creation in such experiments. This is a well-known phenomenon in the field of droplet fluid mechanics. ²⁶ Thus, assessing repeatability between frames or between the eyes is physically unrealistic. We evaluated nearly 8000 frames (8 eyes) and focused on the frames which yielded the smallest droplet diameter. In this study, this diameter was 90 µm and was well within the detection limits of the system (24 µm per pixel). An example of such a droplet distribution was provided in Figure 4e.

The iPhone video showed that direct visualization of droplets through surgical microscope or with the naked eye was possible during the advancement of the microkeratome. However, the quantification of the spread distances, droplet diameters and presence of aerosols cannot be performed from the iPhone video itself. However, the minimum viral load required in aerosols to cause a successful transmission of COVID-19 hasn't been established. Theoretically, even a single virus may be sufficient to transmit a respiratory infection.²⁷ The excimer laser ablation plume did not appear to transmit the human immunodeficiency virus (HIV)-infected, herpesvirus-infected and varicella-zoster virus as they did not seem to survive the ablation.^{28,29} Further, there is no report confirming the presence of SARS-CoV-2 in the excimer laser plume and consequently its transmission. Therefore, the SARS-CoV-2 seems unlikely to pose a health hazard via laser ablation in LASIK and SMILE. Further, femtosecond laser flap creation is a safer alternative to microkeratome since there are no oscillating blades involved. Additionally, the results of this study applied to all infectious diseases that have the potential to be transmitted via aerosols and droplets.

After ablation in PRK and application of mitomycin, slow washing of the surface with BSS is recommended as this may lead to droplets/aerosol formation. This needs to be evaluated in future studies. Topical povidone iodine drops prior to LASIK for a contact period of 2 minutes can reduce the effectivity of the SARS-CoV-2 virus below detectable levels. ³⁰ In conclusion, microkeratome assisted LASIK flap creation resulted in generation of droplets. However, it would be too pre-mature to confirm its role in the transmission of the SARS-CoV-2 virus. Though most of the refractive surgery patients belong to the younger age group who may have less mortality, they are more likely to be asymptomatic carriers of the virus. ³¹ Thus, precautions

such as face mask on the surgeon and patient, use of betadine as a potent anti-viral and bacterial disinfectant prior to the surgery²¹ and use of a protective shield between the surgical area and personnel to reduce the risk of transmission, if at all present, should be strictly followed. A limitation of the study was the 2-dimensional nature of analyses. A more refined 3-D analyses of the droplet trajectories may shed more light on the physics of droplet creation by the microkeratome. Another limitation was that only one model of microkeratome was tested as this was the only model available in our hospital and different makes may have different oscillatory settings.

WHAT WAS KNOWN

- The SARS-Cov-2 virus can spread through aerosols and droplets.
- In ophthalmology, procedures exist which may have the propensity to create aerosols and droplets.

WHAT THIS PAPER ADDS

- As the microkeratome oscillated during the flap cut, large droplets measuring greater than 90 µm were created. These droplets could travel up to distances of 1.8 m.
- However, the droplets were too large and will settle down on surface before aerosolization
 could occur, and the risk of aerosolization and transmission via these droplets was very low.
- Adequate precautions should be followed during flap cut with microkeratome.

References

- 1. Accessed on May 30, 2020. https://www.worldometers.info/coronavirus/.
- 2. Astuti I, Ysrafil. Severe Acute Respiratory Syndrome Coronavirus 2 (SARS-CoV-2): An overview of viral structure and host response. Diabetes Metab Syndr 2020;14:407-412.
- 3. World Health Organization. Statement on the second meeting of the International Health Regulations (2005). Emergency Committee regarding the outbreak of novel coronavirus (2019-nCoV). Accessed May16, 2020. https://www.who.int/news-room/detail/30-01-2020-statement-on-the-second-meeting-of-the-international-health-regulations-(2005)-emergency-committee-regarding-the-outbreak-of-novel-coronavirus-(2019ncov)
- 4. Li Q, Guan X, Wu P, Wang X, Zhou L, Tong Y, Ren R, Leung KSM, Lau EHY, Wong JY, Xing X, Xiang N, Wu Y, Li C, Chen Q, Li D, Liu T, Zhao J, Liu M, Tu W, Chen C, Jin L, Yang R, Wang Q, Zhou S, Wang R, Liu H, Luo Y, Liu Y, Shao G, Li H, Tao Z, Yang Y, Deng Z, Liu B, Ma Z, Zhang Y, Shi G, Lam TTY, Wu JT, Gao GF, Cowling BJ, Yang B, Leung GM, Feng Z. Early Transmission Dynamics in Wuhan, China, of Novel Coronavirus-Infected Pneumonia. N Engl J Med 2020;382: 1199-1207.
- van Doremalen N, Bushmaker T, Morris DH, Halbrook MG, Gamble A, Williamson BN, Tamin A, Harcourt JL, Thornburg NJ, Gerber SI, Lloyd-Smith JO, de Wit E, Munster VJ. Aerosol and Surface Stability of SARS-CoV-2 as Compared with SARS-CoV-1. N Engl J Med 2020;382:1564-1567.
- 6. Tellier R, Li Y, Cowling BJ, Tang JW. Recognition of aerosol transmission of infectious agents: a commentary. BMC Infect Dis 2019;19:101.
- 7. Jones RM, Brosseau LM. Aerosol transmission of infectious disease. J Occup Environ Med 2015;57:501–8.
- 8. Lu CW, Liu XF, Jia ZF. 2019-nCoV transmission through the ocular surface must not be ignored. Lancet 2020;395:e39.
- 9. Kumar K, Prakash AA, Gangasagara SB, Rathod SBL, Ravi K, Rangaiah A, Shankar SM, Basawarajappa SG, Bhushan S, Neeraja TG, Khandenahalli S, Swetha M, Gupta P, Sampritha UC, Prasad GNS, Jayanthi CR. Presence of viral RNA of SARS-CoV-2 in conjunctival swab specimens of COVID-19 patients. Indian J Ophthalmol 2020;68:1015-1017.

- 10. Statista. Number of LASIK surgeries in the United States from 1996 to 2020. Statista; 2019. Accessed May 30, 2020. https://www.statista.com/statistics/271478/ number-of-lasik-surgeries-in-the-us/
- 11. Tasman W, Jaeger EA. Duane's Ophthalmology. Philadelphia, USA, Lippincott Williams & Wilkins. 2009.
- 12. Fang TP, Lin HL, Chiu SH, Wang SH, DiBlasi RM, Tsai YH, Fink JB. Aerosol Delivery Using Jet Nebulizer and Vibrating Mesh Nebulizer During High Frequency Oscillatory Ventilation: An In Vitro Comparison. J Aerosol Med Pulm Drug Deliv. 2016;29:447-453.
- 13. Tang JW-T, Settles G. Images in clinical medicine. Coughing and masks. N Engl J Med. 2009 Dec 24;361: e62.
- 14. Tang JW, Liebner TJ, Craven BA, Settles GS. A schlieren optical study of the human cough with and without wearing masks for aerosol infection control. J R Soc Interface. 2009 Dec 6;6 Suppl 6: S727-736.
- 15. Global alliance of eye bank associations. ALERT UP-DATE: Coronavirus (COVID-2019) and Ocular Tissue Donation. Accessed Nay 22, 2020. http://www.gaeba.org/wpcontent/uploads/2020/03/EBAI_COVID-19-Guidelines 21032020.pdf
- 16. Sengupta S, Dhanapal P, Nath M, Haripriya A, Venkatesh R. Goat's eye integrated with a human cataractous lens: A training model for phacoemulsification. Indian J Ophthalmol 2015;63:275-7.
- 17. Abania N, Reitz RD. Unsteady turbulent round jets and vortex motion. Physics of Fluids 2007;19,125102.
- 18. Schlichting H, Gersten K. Boundary layer theory. 8th Edition. Berlin/Heidelberg, Germany, Springer-Verlag, 2017.
- 19. Sirignano WA. Fluid Dynamics and transport of droplets and sprays. Cambridge, United Kingdom, Cambridge University Press, 1999.
- 20. Wong RS, Banerjee P, Kumaran N. Aerosol generated procedure in intraocular surgery. Accessed May 28, 2020. https://www.youtube.com/watch?v=0pjkNFwIHCA
- 21. Darcy K, Elhaddad O, Achiron A, Keller J, Leadbetter D, Tole D, Liyanage S. Aerosol during phaco (cataract surgery). How to make cataract surgery safe during Covid-19.

- Accessed May 22, 2020. https://www.youtube.com/watch?v=8LGwI9LIYmU&feature=youtu.be
- 22. Tropea C, Yarin A, Foss JS. Handbook of Experimental Fluid Mechanics. Berlin/Heidelberg, Germany, Springer-Verlag, 2007.
- 23. Gralton J, Tovey E, McLaws ML, Rawlinson WD. The role of particle size in aerosolised pathogen transmission: a review. J Infect 2011;62:1-13.
- 24. Manish M, Sahu S. Analysis of droplet clustering in air-assist sprays using Voronoi tessellations. Physics of Fluids 2018;30:123305.
- 25. Wilkinson PS, Davis EA, Hardten DR. LASIK. Ophthalmology. 3rd edition. Missouri, USA, Mosby, 2008.
- 26. Chaudhuri S, Basu S, Kabi P, Unni V, Saha A. Modeling the role of respiratory droplets in Covid-19 type pandemics. Physics of Fluid, 2020; doi:10.1063/5.0015984.
- 27. Nicas M, Nazaroff WW, Hubbard A. Toward understanding the risk of secondary airborne infection: emission of respirable pathogens. J Occup Environ Hyg 2005;2:143-154.
- 28. Taravella MJ, Weinberg A, Blackburn P, May M. Do intact viral particles survive excimer laser ablation? Arch Ophthalmol 1997;115:1028-1030.
- 29. Hagen KB, Kettering JD, Aprecio RM, Beltran F, Maloney RK. Lack of virus transmission by the excimer laser plume. Am J Ophthalmol 1997;124:206-211.
- 30. Kariwa H, Fujii N, Takashima I. Inactivation of SARS coronavirus by means of povidone-iodine, physical conditions and chemical reagents. Dermatology 2006;212 Suppl 1(Suppl 1):119-123.
- 31. Hospitalization Rates and Characteristics of Patients Hospitalized with Laboratory-Confirmed Coronavirus Disease 2019 COVID-NET, 14 States, March 1–30, 2020. Accessed June 23, 2020. https://www.cdc.gov/mmwr/volumes/69/wr/mm6915e3.htm

View publication stats

Figure Legends

<u>Figure 1</u>: Experimental Set up: (a) Set up of Goats eye on a stand; (b) advancement of One-Use Plus SBK Moria microkeratome over the wet corneal surface.

<u>Figure 2</u>: Imaging Technique: (a) Optical set up for high-speed shadowgraphy using CCD camera on the right and a high-power light source on the left; (b) The Mini-UX100 (high speed CCD camera) coupled with a macro lens (ATX 100, 100 mm, f2.8D).

<u>Figure 3</u>: Clinical and shadowgraphy images of an enucleated goat eye mounted on a stand: (a) clinical photo showing droplet generation upon advancement of One-Use Plus SBK Moria microkeratome over the wet corneal surface; (b) high speed shadowgraphy image showing shadows of droplets released during flap creation.

Figure 4: (a) Side-view shadowgraph of the experiment set-up before commencing the microkeratome; (b) Superimposed images of the imaged area during the procedure illustrate the droplet trajectory. Here, x was the horizontal distance travelled by the droplet; (c) Magnified image showing droplets of different sizes; (d) droplet size distribution presented as a histogram; (e) computed value of x from the drag equation plotted against the droplet diameter, D (in μm).

<u>Video Legend</u>: The video shows a split screen of droplet generation during the advancement of One-Use Plus SBK Moria microkeratome over the wet corneal surface in an enucleated goat eye mounted on a stand. Right half of the video frame shows the atomization of water droplets on high-speed shadowgraphy. Left half of the video frame shows a video captured on iPhone 11 Pro (Apple Inc., Cupertino, USA) and the right half shows the shadowgraphy video captured simultaneously.